Repository Istituzionale dei Prodotti della Ricerca del Politecnico di Bari

Graphene-based fine-tunable optical delay line for optical beamforming in phased-array antennas

(Article begins on next page)

20 April 2024

This is the author's final version of the paper published as:

The publisher's version is available at

Graphene-based fine-tunable optical delay line for optical beamforming in phased-array antennas

TERESA TATOLI, DONATO CONTEDUCA, FRANCESCO DELL'OLIO,

CATERINA CIMINELLI*, MARIO N. ARMENISE

Optoelectronics Laboratory, Politecnico di Bari, 70125 Bari, Italy
*Corresponding author: caterina.ciminelli@poliba.it

The design of an integrated graphene-based fine-tunable optical delay line on silicon nitride for optical beamforming in phased-array antennas is reported. A high value of the optical delay time (τg = 920 ps) together with a compact footprint (4.15 mm^2) and optical loss < 27 dB, make this device particularly suitable for a highly efficient steering in active phased-array antennas. The delay line includes two graphene-based Mach-Zehnder interferometer switches and two vertically-stacked microring resonators between which a graphene capacitor is placed. The tuning range is obtained by varying the value of the voltage applied to the graphene electrodes, which controls the optical path of the light propagation and, therefore, the delay time. The graphene provides faster reconfigurable time and low values of energy dissipation. Such significant advantages, together with negligible beam-squint effect, allow to overcome the limitations of the conventional RF beamformers. A highly efficient fine tunable optical delay line for the beam steering of 20 radiating elements up to ±20° in the azimuth direction of a tile in a phased-array antenna of an X-band SAR has been designed. © 2016 Optical Society of America

1. INTRODUCTION

Optical delay lines are attracting a rising scientific interest due to their inherent advantages such as compact footprint, wide bandwidth and low power consumption, and to their crucial role assumed in several applications, such as information processing, communications, and microwave photonics (MWP). In telecommunication and information processing, they are often used for synchronization, buffering and storage of wideband data stream [1]. High-speed optical delay lines are essential to achieve real time imaging in optical coherence tomography (OCT) [2], and they are also key elements for reconfigurable filters, oscillators, correlators and beamformers in MWP field [3-6]. In particular, True Time Delay (TTD) beamforming provides the steering function in active Phased-Array Antennas (PAA), through progressive differential time delay in the excitation of the radiating elements [5].

A remarkable advantage of TTD lines concerns negligible beam-squint effect, so preventing the distortion of the radiating beam, which is a critical issue of the conventional RF beamformers based on phase-shifters (i.e. switched line, loaded line, traveling wave and vector modulated based phase shifters) [5,7]. Further advantages of integrated technologies for optical devices are related to volume and mass reduction, immunity to electromagnetic interference, and low transmission loss.

Since early 90s, many configurations of optical beamformers have been proposed in literature, based on discrete optics [8], fiber optics [9-12], and integrated optics [13-19].

Several integrated optical delay lines have been proposed in literature based on different configurations, such as spiral waveguides [20], gratings [21-23], ring resonators [24], and photonic crystals [25].

High values of time delay, while preserving a compact footprint, have been demonstrated by using long spiral waveguides. In [20] a 7 m long spiral waveguide on a silicon chip, with a diameter equal to 4 cm, is reported, allowing a delay higher than 30 ns and a loss less than 0.1 dB/m.

A delay line based on an apodized grating realized on silicon-on-insulator rib waveguides has been proposed in [21]. The structure, of length equal to 2 cm, incorporates a pn junction on which a forward voltage is applied in order to achieve a continuous tunability up to 660 ps. A loss per unit delay equal to 3.3 dB/ns is reported.

An enhancement of the manipulation of the light dispersion properties has been obtained with resonant cavities [26], but at the expenses of the bandwidth [27].

In [28] a grating-assisted contradirectional coupler with a length equal to 3.72 mm has been realized on SOI technology. A fine-tunable delay

from 21 ps to 96 ps can be achieved exploiting the thermo-optic effect with a power efficiency equal to 11 mW/ps. The loss per unit delay is 20 dB/ns, mainly due to sidewall scattering.

The delay lines consisting of the cascade of several ring resonators in All Pass Filter (APF) and Coupled Ring Resonator Optical Waveguide (CROW) configurations were investigated in [29-30]. The ring resonators in CROW and APF configurations proposed in [30] are manufactured in silicon wire with a radius of 6.5 μm. The CROW includes 100 elements, achieving a fixed delay of 220 ps with an attenuation of 23 dB, while the APF delay line, consisting of 56 elements, arranged within an area of about 0.09 mm^2, provides a fixed delay equal to 510 ps and an attenuation of 22 dB. In [29] a thermo-optically reconfigurable delay line in silicon oxynitride (SiON) waveguide has been demonstrated. This delay line includes a CROW structure, which acts as a discrete delay section, followed by a ring resonator phase shifter that adds fine tuning. The discrete variation of the delay is achieved by tuning at resonance the proper number of resonators by means of the thermo-heater placed on each ring. The power required by every thermo-heaters is about 12 mW/GHz, so a shift of twice the FWHM (~6 GHz) requires a power equal to 72 mW. With four resonators tuned at resonance, a delay of 800 ps has been experimentally measured with an attenuation of about 8 dB.

Photonic crystals have been also investigated to realize high efficient optical delay lines, but with the drawback of tighter fabrication tolerances. A delay time up to 200 ps has been achieved by properly engineering the dispersion of line defect waveguide [25]. Moreover, a Photonic Crystal Coupled Cavity Waveguide (PC-CCW) was proposed that can reach a delay time as high as 12 ns, with a footprint of a few millimetres [31].

Discrete optical delay lines can only allow discrete beam-steering, which is not adequate for phased array antenna used in SAR for Earth Observation. Such devices are usually realized by a switched architecture to allow optical path changes, so involving a delay time variation [16,32]. In particular, delay lines based on fiber grating prism [9] or photonic crystal waveguides [25, 19], exploit the resonance shift in order to achieve different discrete time delays.

The fine tuning capability is a crucial aspect of an optical delay line used for beamforming applications. An example of a continuously tunable delay network for beamforming application is proposed in [17]. Such device is based on ring resonators in APF configuration arranged in a binary tree topology. The delay introduced by a single ring resonator can be tuned by using a thermo-optic heater integrated on each ring. The major drawback of this configuration is the system complexity. The combination of a discrete delay section, having fixed delay step Δτ, with a second continuously delay section which allows the fine tuning of the delay up to Δτ, represents the most suitable solution to overcome the limitation of discrete delay lines. Such approach has been exploited by several integrated structures, such as spirals [15], CROWs [29], and also optical fibers [12]. The thermo-optic technique is the most used approach to obtain the tunability of the delay time. This is an efficient and mature tuning method that allows a high range of tunability, although at the expenses of a slow response time (> 10 μs) [33]. Moreover, it is difficult to control locally the temperature rise [21]. The electro-optic tuning method is much faster, even providing a switching time of the order of nanoseconds, and also allowing a very compact device footprint. However, this approach is typically affected by higher values of absorption loss, thus requiring proper design and manufacturing technique to limit losses.

In the last years, electro-optic tuning based on the graphene integration in optoelectronic components has demonstrated the feasibility of realizing extremely fast and broadband electro-optically tunable optical devices [34-36].

Graphene is a monolayer of carbon atoms arranged in a two dimensional honeycomb lattice. It is a zero gap material with very attractive properties: linear dispersion, vanishing rest mass, large carrier mobilities (up to 200000 cm^{2}V^{-1}s^{-1}, in suspended graphene), and very good thermal and mechanical features.

Its extraordinary properties in terms of high conductivity and optical transparency, make graphene particularly suitable to realize transparent charge injecting electrodes in organic light-emitting diodes (OLEDs), or conducting films in touch screens, optical polarizer, mode locked laser, photodetector, optical switches and modulators [37-39]. Microwave photonic devices based on graphene, such as filters, phase shifters and delay lines, have been also proposed in literature [40].

Graphene-based electro-optically tunable optical delay lines have been proposed with PhC cavities [41] and microring resonators [42]. High values of maximum delay time of about 200 ps and 250 ps have been obtained with microring resonators in CROW and APF structures, respectively, with a footprint smaller than 10^5 mm^2. The delay time is tuned electro-optically, with a very fast reconfiguration time of about 0.12 ns, which is five orders of magnitude faster than typical values obtained with thermo-optic effect [33].

In this paper, we report on the design of a new graphene-based fine tunable optical delay line on silicon nitride (Si$_3$N$_4$) platform to be used as the key element in a beamforming network for the PAA of an X-band Synthetic Aperture Radar (SAR). The optical delay line is formed by the cascade of two Mach-Zehnder interferometric (MZI) switches and two graphene-based vertically-stacked microring resonators, as described in the next section. The graphene integration in the delay line allows an electro-optical tunability. A tunable delay line with a differential delay time up to $\Delta\tau_g$ = 920 ps, together with a reduced footprint of about 4.5 mm^2, optical loss α < 27 dB, reduced energy consumption and fast reconfiguration time has been designed. This device appears to be particularly useful for the steering of the transmitted/received beams in a PAA tile, comprising 20 radiating elements, operating at the central frequency $f_c = 1/\lambda_c$ =9.65 GHz and equally spaced by 0.7 λ_c, at an azimuthal angle of ±20°, which is consistent with the application of a SAR for Earth Observation [43].

2. DEVICE CONFIGURATION

The configuration of the delay line includes a first section with two cascaded spiral waveguides and two MZI switches, which provides a discrete value of the delay time, and a second section with two vertically-stacked microring resonators to obtain a fine tunable differential delay, as shown in Fig. 1. The graphene integration in the switches and between the stacked microrings allows the realization of the graphene capacitors responsible for the electro-optical tuning.
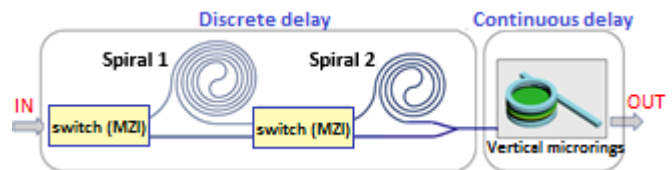

Fig. 1. Configuration of the graphene-based optical delay line.

Silicon nitride technology has been chosen as the most suitable for the design of the optical delay line, due to the fabrication of very low loss waveguides [44,45] and also to possibility of realizing vertically-stacked microring resonators [46,47]. Furthermore, radiation hardness tests carried out on silicon nitride structures have confirmed that there is no refractive index change after radiation, so demonstrating the suitability of this technology also for space applications [48].

Each element of the optical delay line (see Fig. 1) is based on a Si$_3$N$_4$ (n$_{Si3N4}$ = 1.98) waveguide with a width of w = 900 nm and a height of h =

644 nm [45], totally embedded in a silicon dioxide (n_{SiO2} = 1.45) cladding.

Graphene capacitors are formed over one arm of each MZI and above the lower ring of the vertically-stacked resonant structure. These capacitors include two graphene monolayers (electrodes) with a thickness t = 0.35 nm and a layer of dielectric material, alumina (Al$_2$O$_3$), with a thickness s = 10 nm [49]. The graphene monolayer can be fabricated by Chemical Vapour Deposition (CVD), due to its feasibility to obtain large and high quality area [50]. The same technique can also be used for the deposition of the Al$_2$O$_3$ film and the second monolayer of graphene, which is placed on top of the alumina. The whole cavity is fully embedded in silica.

The device proposed in Fig. 1 is a switched optical delay line, in which the incoming signal can be transmitted through different optical paths in the first section, thus achieving different discrete delays. The graphene-based MZI switches can route the incoming signal to the spiral waveguides, with a delay proportional to their length, or to the straight waveguides, where delay is much lower. The first section provides a discrete tunability of the optical delay time, as a function of the path in which the light propagates. The two vertically-stacked microring resonators in the second section provide a fine tunability to obtain a total delay time of the device of about 1 ns.

Such performance makes the on-chip graphene-based optical delay line well suitable in optical beamforming networks, where high values of differential delay time and a wide continuously tuneable range are required, so enabling a tight control on the steering angle of the PAA radiation.

3. DESIGN AND NUMERICAL RESULTS

A. Discrete delay time section

The spiral waveguides have been designed as two interleaved Archimedean spirals with S-bend connections [51], as shown in Fig. 2. We have calculated by FEM simulations the value of group index n_g = 2.07 for the fundamental quasi-TE mode in the Si$_3$N$_4$ waveguide at λ = 1550 nm. The spirals have different lengths to provide different delay time, according to τ_g = (L·n_g)/c, where L is the length of the spiral and c the velocity of light. The results obtained by 2D FEM simulations have demonstrated that a curvature radius equal to 100 μm for each S bend ensures negligible bending loss and a separation between neighbouring waveguides in the spirals set at 3 μm prevents any coupling effect between them. Thus, the first spiral resulted with a length equal to L$_1$ = 67 mm with 39 coils and an external radius of about 352 μm, in order to achieve a delay time τ_{g1} = 460 ps; the second one has a length L$_2$ = 33.5 mm with 22 coils and the external radius of about 286 μm, so providing τ_{g2} = 230 ps, which is exactly half the delay of the first spiral. Considering the intrinsic attenuation coefficient of 0.12 dB/cm in the Si$_3$N$_4$ waveguide, which includes scattering and absorption losses [45], and neglecting the bending losses (< 10^{-2} dB/cm), the total optical loss α = 0.8 dB and α = 0.4 dB have been calculated for long and short spirals, respectively.
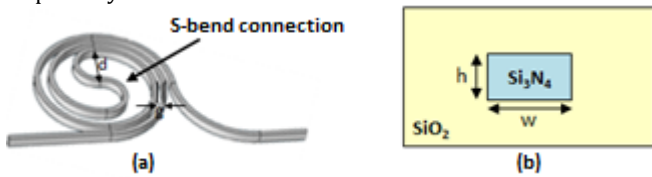

Fig. 2. (a) Spiral waveguide configuration with a length L, a diameter of S-bend connection d = 200 μm and a separation between neighboring waveguides g = 3 μm. (b) Cross-section of the Si$_3$N$_4$ waveguide

embedded in silica, used to realize the spiral with width w = 900 nm and height h = 644 nm [45].

Two graphene-based MZI switches have been used to reconfigure the optical path of the signal. Each switch has two 207 μm long 3-dB coupler and a graphene capacitor, as shown in Fig. 3. The couplers are constituted by curved waveguides having bending radius equal to 100 μm, and coupling sections with a length of about 12 μm in which the two coupling waveguides are separated by 600 nm, to obtain a perfect power splitting in both arms of the MZI. The graphene capacitor on one arm of the MZI switch has been designed to manipulate the optical power at the outputs. The graphene capacitor has been placed 240 nm above the Si$_3$N$_4$ waveguide, because of the requirement of the vertically-stacked microring resonator to avoid the resonance splitting, as discussed in the next section.
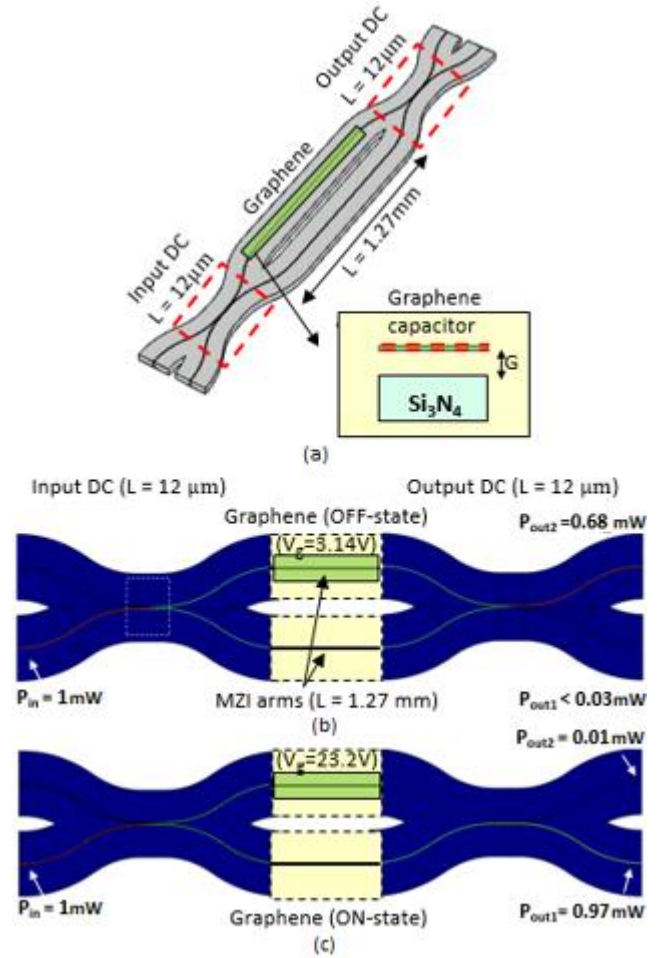

Fig. 3. (a) Configuration of the graphene-based MZI switch; the inset shows the graphene capacitor placed above the Si$_3$N$_4$ waveguide, with G = 240 nm. (b) 2D FEM simulations of the graphene-based MZI in OFF-state with V_g = 3.14 V; (c) in ON-state with V_g = 23.2 V.

Assuming the light enters the lower arm of the switch, a length L = 1.27 mm of the MZI arm is necessary to obtain the total power in the top waveguide at the output, according to P_{out2} = $P_{in}\cos^2(\Delta\Phi/2)$, when ΔΦ = Δβ·L = 0. The presence of undoped graphene capacitor on one arm of the switch causes a change of the effective index between the arms, which corresponds to an undesired asymmetry in the structure with an uncompleted power exchange. It is necessary to apply a voltage across the graphene electrodes to obtain a shift of the graphene Fermi level, so providing the same effective index for both the waveguides (n_{eff} =

1.7032). The symmetry condition has been calculated by assuming μ_c = 0.42 eV.

The relationship between the graphene chemical potential μ_c and the applied voltage V_g across the electrodes is:

$$\mu_c(V_g) = \hbar v_F \sqrt{\pi \frac{C'}{e} |V_g - V_0|} \qquad (1)$$

where $\hbar$ is the reduced Plank constant, v_F is the Fermi velocity, $C' = \varepsilon_0 \varepsilon_{Al2O3}/s$ is the effective capacitance per unit area with ε_{Al2O3} = 10, e is the electron charge and V_0 (= 0.8 V) is the offset voltage for the natural doping.

An applied voltage V_g = 3.14 V is necessary to provide μ_c = 0.42 eV, according to Eq. 1, so obtaining the condition $\Delta\Phi = 0$ with a total power transfer from the input waveguide to the top one at the output of the MZI switch, as confirmed by 2D FEM simulations (see Fig. 3b).

The mathematical model proposed in [52] has been used to calculate the graphene optical conductivity σ and the relative permittivity given by $\varepsilon = 1 + i\sigma/\omega\varepsilon_0 t$, where ω is the angular frequency and t the thickness of the graphene monolayer. An effective index n_{eff} = 1.7032-i8.53x10^{-5} has been calculated for μ_c = 0.42 eV, which corresponds to the graphene loss α = 30 dB/cm, obtained by applying V_g = 3.14 V between the graphene electrodes with a length L = 1.27 mm. A slight doping of graphene corresponds to high values of optical loss in the corresponding arm of the MZI. Assuming an input power of 1 mW at the lower waveguide, with V_g = 3.14 V the optical power calculated at the output from the top waveguide is P_1 = 0.68 mW and P_2 < 0.03 mW from the bottom one, which corresponds to a total optical loss of each MZI switch α = 1.67 dB.

The power transfer changes with different values of the applied voltage on the graphene-capacitor. The phase shift $\Delta\Phi = \pi$, which corresponds to the maximum power at the output in the same bottom waveguide with a minimum power exchange condition in the MZI switch, has been calculated with μ_c = 1.30 eV. Such condition corresponds to an applied voltage V_g = 23.2 V, for a length of the MZI arm L = 1.27 mm. In this case, an effective index n_{eff} = 1.7026-i4.80x10^{-7} has been obtained, which corresponds to an optical loss α in that MZI arm of 0.17 dB/cm, taking into account also the scattering and the absorption loss of the waveguide. An effective index change Δn_{eff} = 6x10^{-4} has been calculated, which corresponds to the condition of the minimum power exchange, obtaining an output power P_1 = 0.01 mW in the same waveguide and P_2 = 0.97 mW in the lower one. The transparency condition of graphene obtained with μ_c = 1.3 eV corresponds to an optical loss α < 0.2 dB at the output of the MZI switch.

The insertion loss of the switch depends on its operating conditions. In fact, as already mentioned, the bar state of the switch is obtained for μ_c = 1.30 eV while the cross state is achieved for μ_c = 0.42 eV. For μ_c = 1.30 eV the graphene is transparent at the operating wavelength and consequently the switch loss in the bar state is very low (< 0.2 dB). For μ_c = 0.42 eV the graphene is not transparent at the operating wavelength. Therefore, in the cross state the switch loss increases up to 1.67 dB.

The energy consumption necessary to obtain the switching of optical power from the top waveguide to the bottom one is given by:

$$E_{switch} = \frac{1}{2} C(V^2_{ON} - V^2_{OFF}) \qquad (2)$$

where C is the capacitance, V_{ON} (= 23.2 V) and V_{OFF} (= 3.14 V). A capacitance C = 10.1 pF has been calculated with an area of the graphene electrodes of 1.1x10^{-3} mm^2, corresponding to E_{switch} ~ 2.7 nJ.

B. Fine tuneable delay time section

The two vertically-stacked microring resonators represent the last key element of the optical delay line to obtain a fine tunable delay time. The configuration, already proposed in [46], includes two vertically coupled Si$_3$N$_4$ microring resonators with the same radius of 20 μm. The graphene-based capacitor has the same structure of those of the MZI switches, with two graphene monolayers (t = 0.35 nm) and an alumina layer with s = 10 nm as electrodes and dielectric, respectively. It is placed exactly in the middle of the vertical gap between the microring resonators to manipulate the coupling condition, as shown in Fig. 4a. The graphene structure is on the same plane of the capacitors used in the other optical devices, so simplifying the device manufacturing with a decrease of the fabrication steps.
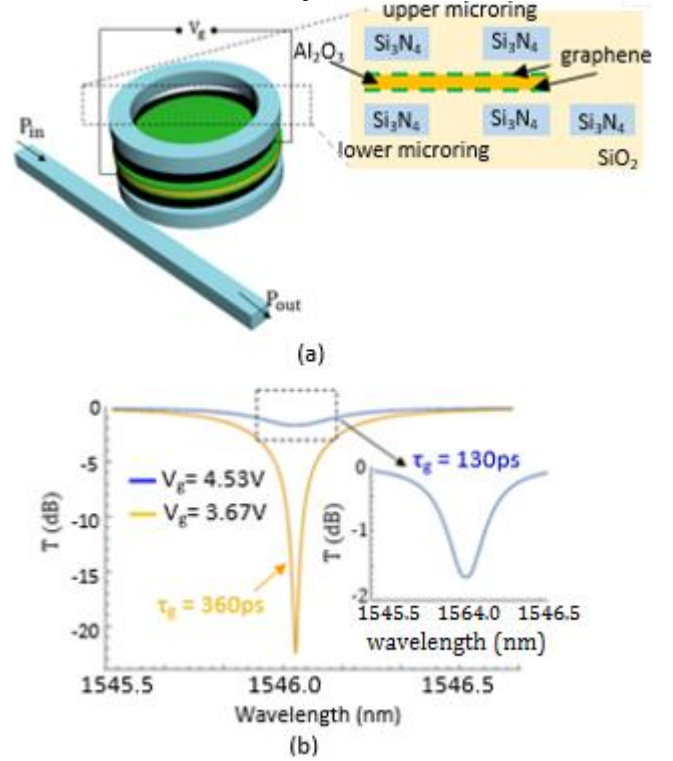

Fig. 4. (a) Configuration of the graphene-based vertically-stacked microring resonators with a radius R = 20 μm. The inset shows the device cross-section with the graphene capacitor placed in the middle of the vertical gap between ring resonators (G = 240 nm). (b) Transmission spectra of the resonant cavity for two different values of the applied voltage to the graphene electrodes to provide a differential delay time $\Delta\tau_g$ = 230 ps [46].

The design of the vertically-stacked microring resonators has been already discussed in [46]. A vertical gap of 480 nm is necessary to avoid the resonance splitting, which corresponds to a distance G = 240 nm between the graphene-capacitor and the lower microring. The graphene electrodes have been assumed to cover only the microring resonators with an annulus shape and area of 110 μm^2.

The applied voltage on the graphene capacitor is changed to obtain the fine tuning of the optical delay time. A transparent condition has been assumed for the vertically-stacked microring resonators with a chemical potential μ_c = 0.53 eV, which corresponds to an applied voltage V_g = 4.53 V, as given by Eq. 1. Under this condition, a Q-factor of 6.4x10^3 with a resonance condition at λ = 1546.05 nm has been calculated, with an extinction ratio ER = 1.7 dB and an optical delay time τ_g = 130 ps (see Fig. 4b). A decrease of the applied voltage provides an increase of the optical loss in the cavity, which also corresponds to higher values of delay time [46].

Even if the vertically-stacked microring resonators introduce a fixed minimum delay time of 130 ps, it does not represent a critical issue for the target application chosen for proposed device, because only the

differential delay between two consecutive radiating elements affects the beam steering in a specific direction.

Since the minimum time step of the discrete delay section is $\Delta\tau_g = 230$ ps, in order to assure the fine tunability of the overall delay line, the graphene-based vertically-stacked microring resonators have been designed to provide such differential delay time.

Taking into account a minimum delay time of 130 ps, calculated with $\mu_c = 0.53$ eV, that is the condition of transparency for graphene, it has been observed that a chemical potential $\mu_c = 0.465$ eV is necessary to obtain $\tau_g = 360$ ps, so fulfilling the condition $\Delta\tau_g = 230$ ps for a fine tuning of the optical delay line. The value of the chemical potential $\mu_c = 0.465$ eV has been obtained by assuming an applied voltage $V_g = 3.67$ V, which corresponds to a Q-factor of $7\mathrm{x}10^3$ and an extinction ratio ER = 23 dB for the resonant cavity, as shown in Fig. 4b.

In the vertically-stacked microring resonators, the delay tuning is achieved by the voltage-induced change in the real part of the graphene refractive index. Since in the graphene layer any change of the real part implies a variation of the imaginary part, the delay tuning induces also a variation of the insertion loss.

This range of tunability in the vertically-stacked microring resonators corresponds to a total energy consumption $E_{switch} = 3.4$ pJ and a switching time $t_s < 2$ ns with a total footprint of $1.6\mathrm{x}10^3$ μm^2, as calculated in [46].

C. Overall performance of the optical delay line

The performance of the optical devices included in the optical delay line have been discussed in the previous sections. Here, a description of the overall behavior of the optical delay line, in terms of delay time, optical loss and footprint, is reported.

The minimum delay time has been obtained when the light does not propagate in the spiral waveguides, which is obtained assuming an OFF condition for the first MZI switch and an ON-state for the second one, (see Fig. 4 (b), (c)) assuming an input power $P_{in} = 1$ mW in the bottom waveguide. This condition can be obtained by applying the voltage $V_{OFF} = 3.14$ V on the graphene of the first MZI, which corresponds to an optical loss $\alpha = 1.67$ dB, and $V_{ON} = 23.2$ V with $\alpha = 0.2$ dB for the second switch. A differential delay time $0 \leq \Delta\tau_g \leq 230$ ps, as a function of the applied voltage across the graphene capacitor of the vertically-stacked microring resonators, can be obtained if the light propagates in the straight waveguide for both paths. In this case, the optical loss is in the range 3.6 dB $\leq \alpha \leq$ 24.9 dB, depending on the tunable voltage on the vertically-coupled microrings.

If the MZI switches are both set in the OFF-state, then a crossing condition is achieved, which corresponds to the light propagation only in the short spiral, as shown in Fig. 5a. Therefore, an optical delay time in the range $230 < \Delta\tau_g < 460$ ps has been calculated, because a fixed delay time of 230 ps is given by the propagation in the shorter spiral and a fine tuneable delay from $\Delta\tau_g = 0$ ps to $\Delta\tau_g = 230$ ps is allowed by the vertically-coupled microrings. The optical loss calculated is 5.5 dB $< \alpha <$ 26.8 dB, as shown in Fig. 5a.

Moreover, if only the first MZI switch is ON, the light propagates only in the longer spiral and the minimum delay time is $\Delta\tau_g = 460$ ps, which corresponds to a low optical loss $\alpha \leq 4.4$ dB. The maximum delay is $\Delta\tau_g = 690$ ps when the vertically stacked microring resonators are in ON-state, corresponding to $\alpha \leq 25.7$ dB.

Finally, when both the MZI switches are in ON-state, the light propagates in both spirals, so obtaining $690 < \Delta\tau_g < 920$ ps, as shown in Fig. 5b. In this case, the optical loss is $\alpha \leq 24.6$ dB, as a function of the applied voltage on the vertically-coupled microrings.

The results confirm a fine tuneable optical delay time up to $\Delta\tau_g = 920$ ps with total optical loss $\alpha \leq 27$ dB.

Since it is not possible to decouple the electrabsorptive and the electrorefractive effects in the graphene layer, the device loss depends on the required delay. To solve this critical aspect, the loss could be properly compensated by an amplification that should be tuned accordingly to the delay. This approach implies the use of an optical amplifier with a tunable gain at the device output and a properly designed electronic circuit regulating both the delay and the compensating amplification.

In Tab. 1, a comparison between the performance of the proposed delay line and the state-of-the-art of integrated optical delay lines has been reported. The delay lines based on SOI technology have the lowest footprint, which also corresponds to the highest ratio of the achievable delay time to the occupied area (τ_g/A). In particular, a value $\tau_g/A = 5.7$ ns/mm^2 in [30] and τ_g/A up to 9.58 ns/mm^2 for the thermo-optic continuously tunable delay line reported in [33] have been obtained. Since both these delay lines are based on ring resonators in APF configuration, they are characterized by a high attenuation, equal to 43 dB in the case of the 56 ring resonators reported in [30] and 14 dB in the case of the 20 ring resonators in [33]. Silicon OxyNitride (SiON) technology provides lower optical losses, as verified in [29] with a device including 4 racetrack resonators in CROW configuration, where low loss equal to 8 dB for 800 ps of delay has been achieved. A further decrease of optical losses can be achieved by considering lower values of index contrast of optical waveguides such as those based on silica [15] and silicon nitride technology [16,24]. In particular, the delay line reported in [16], which comprises 4 spirals in Si$_3$N$_4$ with MZI thermo-optic switch provides a maximum delay time up to 12.35 ns with a very-low optical loss $\alpha = 2.43$ dB, but at the expense of the device footprint (A = 38 cm^2) and also a discrete tunability with a resolution of delay time of 0.85 ns, which makes unsuitable such device for SAR application. A similar behavior has been observed in [24] where a delay line in Si$_3$N$_4$ technology allows a maximum delay of 632 ps with a low attenuation of 5.3 dB, but with the advantage of a continuous tunability by using the thermo-optic approach.

The proposed graphene-based delay line ensures a continuously tunable delay up to 920 ps with a small device footprint A = 4.15 mm^2, corresponding to a figure of merit $\tau_g/A = 0.22$ ns/mm^2. The ratio between the maximum delay and the occupied area is equal to 0.22 ns/mm^2, much higher than the values obtained by the other delay lines based on silica or silicon nitride technology, but lower than performance of delay lines in SOI technology, which, however, typically provide lower values of delay time. The electro-optical tuning is typically affected by higher values of optical losses, as confirmed by the obtained values of $\alpha < 27$ dB and a figure of merit $\alpha/\tau_g = 29$ dB/ns, which is more than one order of magnitude higher than the corresponding value obtained by using a thermo-optical approach with delay lines in the same technology. However, the most relevant advantage of such tuning approach is related to very low response time of about few nanoseconds and low energy consumption with compact device footprint.

The proposed fine tunable delay line can be used to implement a beamforming network for a PAA used in X-band SAR for Earth Observation. The target application is the beamsteering of the radiation of a tile, comprising 20 radiating elements operating at the central frequency of 9.65 GHz. The differential delay time $\Delta\tau_g = 920$ ps is suitable to control the radiation up to a maximum steering angle of about ±20°, which is consistent with the application of a SAR for Earth Observation.
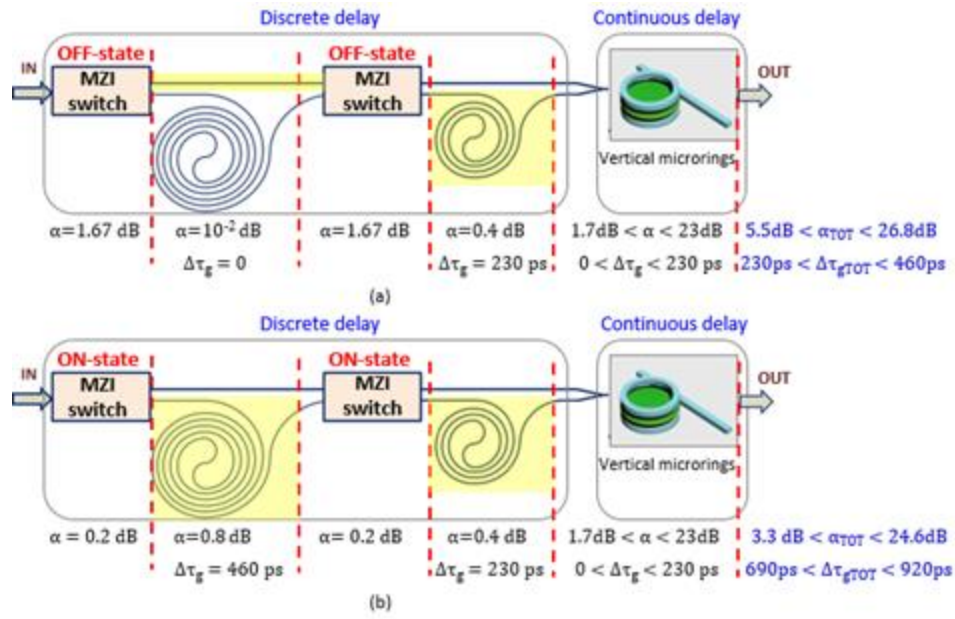
Fig. 5. Configuration of the optical delay line with (a) both MZI switches in OFF-state to obtain an optical delay time 230 ps < $\Delta\tau_g$ < 460 ps with an optical loss 5.5 dB < α < 26.8 dB, and (b) both MZI switches in ON-state, providing 690 ps < $\Delta\tau_g$ < 920 ps and optical loss 3.3 dB < α < 24.6 dB. An input power P_{in} = 1 mW has been assumed in the bottom waveguide.

Table 1. State-of-the-art of integrated optical delay lines.

Configuration	Tech.	Tuning mechanism	Max. time delay τ_g [ns]	Area [mm²]	Loss α [dB]	τ_g/A [ns/mm²]	α/ τ_g [dB/ns]	Power [mW]	Resp. time
56 ring resonators in APF [30]	SOI	Fixed delay line	0.51	0.09	22	5.7	43	-	-
4 spirals with MZI switch [16]	Silicon nitride	Thermo-optic (Discrete with	12.35	38.25x10²	2.43	3.2x10⁻³	0.19	1040	> 1 ms
4 spirals and 4 cascaded ring resonators [15]	Silica	Thermo- optic (continuous)	2.56	12x10²	3.38	2.1x10⁻³	1.32	-	-
4 racetrack resonators [29]	SiON	Thermo-optic (continuous)	0.8	5	8	0.16	10	288	< 1 ms
20 racetrack resonators [33]	SOI	Thermo-optic (continuous)	0.345	~0.036	14	~9.58	40.57	-	< 10 μs
40 racetrack resonators [24]	Silicon nitride	Thermo-optic (continuous)	0.632	53.29	5.3	1.2x10⁻²	4.74	-	-
Apodized grating waveguide [22]	SOI	Thermo-optic (continuous)	0.22	0.0015	9.3	146.7	42.27	~ 500	
Complementary apodized cascaded grating waveguide [23]	SOI	Thermo-optic (continuous)	0.082	0.003	3.2 dB	27.3	39.02	~ 500	
This paper	Silicon nitride	Electro-optic (continuous)	0.92	4.15	26.8	0.22	29	200	< 2 ns

4. CONCLUSION

The design of an integrated graphene-based continuously tunable silicon nitride (Si_3N_4) delay line has been proposed. The device includes a discrete delay section with two Archimedean spiral waveguides and two MZI switches, which can provide a maximum delay time of 920 ps with a minimum step of delay time of 230 ps. Two graphene-based vertically stacked microring resonators have been designed to obtain a continuous tuning range of optical delay time up to 230 ps, so they have been placed in cascade to the discrete delay section to realize a fine tunable delay line from 130 ps to 1050 ps, which corresponds to a tuning range of 920 ps. Graphene capacitors have been integrated in MZI switches and in the vertically-stacked microring resonators to exploit the advantages of the electro-optical tuning approach, related to fast tunability and low energy consumption. The large tuning range, together with the compact footprint of 4.15 mm^2 and fast reconfiguration time, make the proposed delay line suitable to realize the optical beamforming of a PAA tile of an X-band SAR, thus overcoming the limitations of conventional RF beamformers in terms of occupied area and power consumption. The advantage of the designed device with respect to the delay lines based on other approaches proposed in literature, e.g. the separate carrier tuning technique [40], is the larger maximum delay that it can realize. This key feature has a strong impact on the maximum steering angle if the delay line is used as basic building block in a beamformer for PAAs.

References

1. R.W. Boyd, D.J. Gauthier, and A.L. Gaeta "Applications of slow light in telecommunications," Optics and Photonics News **17**, 18 -23 (2006).
2. C. Rosa, J. Rogers, and A.G. Podoleanu, "Fast scanning transmissive delay line for optical coherence tomography," Opt. Lett. **30**, 3263–3265 (2005).
3. R.A. Minasian, "Photonic Signal Processing of Microwave Signals," IEEE Transactions on Microwave Theory and Techniques **54**, 832-846 (2006).
4. J. Capmany, and D. Novak, "Microwave photonics combines two worlds," Nature Photonics **1**, 319-330 (2007).
5. J. Yao, "Microwave Photonics," IEEE Journal of Lightwave Technology **27**, 314-335 (2009).
6. S. Iezekiel, M. Burla, J. Klamkin, D. Marpaung, and J. Capmany, "RF Engineering Meets Optoelectronics: Progress in Integrated Microwave Photonics," IEEE Microwave Magazine **16**, 28-45 (2015).
7. M. Longbrake, "True time-delay beamsteering for radar," IEEE National Aerospace and Electronics Conference, NAECON 2012; Dayton (USA), 25-27 July 2012.
8. Y. Xiaoke, T.X.H. Huang, and R.A. Minasian, "Photonic Beamforming Based on Programmable Phase Shifters With Amplitude and Phase Control," IEEE Photonics Technology Letters **23**, 1286-1288 (2011).
9. H. Zmuda, and R. A. Soref, P. Payson, S. Johns, E. N. Toughlian, "Photonic beamformer for phased array antennas using a fiber grating prism," IEEE Photonics Technology Letters **9**, 241-243 (1997).
10. Y. Liu, J. Yang, and J. Yao, "Continuous True-Time-Delay Beamforming for Phased Array Antenna Using a Tunable Chirped Fiber Grating Delay Line," IEEE Photonics Technology Letters **14**, 1172-1174 (2002).
11. P. Wu, S. Tang, and D.E. Raible, "A prototype high-speed optically-steered X-band phased array antenna," Optics Express **21**, 32599-32564 (2013).
12. X. Gao, S. Huang, S. Wei, C. Gao, J. Zhou, H. Zhang, and W. Gu, "A high-resolution compact optical true-time delay beamformer using fiber Bragg grating and highly dispersive fiber," Optical Fiber Technology **20**, 478-482 (2014).
13. M.N. Armenise, V.M. N. Passaro, and G. Noviello, "Lithium niobate guided-wave beam former for steering phased-array antennas," Applied Optics **33**, 6194-6209 (1994).
14. M.N. Armenise, M. Armenise, and R. Diana, "Novel integrated optical beam former for phased-array antennas," Proc. SPIE **3464**, 95-103 (1998).
15. M.S. Rasras, C.K. Madsen, M.A. Cappuzzo, E. Chen, L.T. Gomez, E.J. Laskowski, A. Griffin, A. Wong-Foy, A. Gasparyan, A. Kasper, J. Le Grange, and S.S. Patel, "Integrated resonance-enhanced variable optical delay lines," IEEE Photonics Technology Letters **17**, 834-836 (2005).
16. R.L. Moreira, J. Garcia, W. Li, J. Bauters, J.S. Barton, M.J.R. Heck, J.E. Bowers, and D. Blumenthal, "Integrated ultra-low-loss 4-bit tunable delay for broadband phased array antenna applications," IEEE Photonics Technology Letters **25**, 1165-1168 (2013).
17. A. Meijerink, C.G.H. Roeloffzen, R. Meijerink, L. Zhuang, D.A.I. Marpaung, M.J. Bentum, M. Burla, J. Verpoorte, P. Jorna, A. Hulzinga, and W. van Etten, "Novel Ring Resonator-Based Integrated Photonic Beamformer for Broadband Phased Array Receive Antennas - Part I: Design and Performance Analysis," IEEE Journal of Lightwave Technology **28**, 3-18 (2010).
18. L. Zhuang, C.G.H. Roeloffzen, A. Meijerink, M. Burla, D.A.I. Marpaung, A. Leinse, M. Hoekman, R.G. Heideman, and W. van Etten, "Novel Ring Resonator-Based Integrated Photonic Beamformer for Broadband Phased Array Receive Antennas - Part II: Experimental Prototype," IEEE Journal of Lightwave Technology **28**, 19-31 (2010).
19. C.-Y. Lin, H. Subbaraman, A. Hosseini, A.X. Wang, L. Zhu, R.T. Chen, "Silicon nanomembrane based photonic crystal waveguide array for wavelength-tunable true-time-delay lines," Applied Physics Letters **101**, 051101 (2012).
20. H. Lee, T. Chen, J. Li, O. Painter, and K.J. Vahala, "Ultra-low-loss optical delay line on a silicon chip," Nature Communication **3**, 1-7 (2012).
21. S. Khan, M.A. Baghban, and S. Fathpour, "Electronically tunable silicon photonic delay lines," Optics Express **19**, 11780-11785 (2011).
22. S. Khan, S. Fathpour, "Demonstration of tunable optical delay lines based on apodized grating waveguides," Opt. Express **21**, 19538-19543 (2013).
23. S. Khan, S. Fathpour, "Demonstration of complementary apodized cascaded grating waveguides for tunable optical delay lines," Opt. Lett. **38**, 3914-3917 (2013).
24. P.A. Morton, J.B. Khurgin, Z. Mizrahi, and S.J. Morton, "Commercially packaged optical true-time-delay devices with record delays of wide bandwidth signals," CLEO: Applications and Technology, Optical Society of America (2014). Paper AW3P.5.
25. L. O'Faoilain, S. Schulz, D.M. Beggs, T.P. White, A. Di Falco, A. Samarelli, M. Sorel, R.M. De La Rue, F. Morichetti, A. Canciamilla, A. Melloni, and T.F. Krauss, "Low loss dispersion engineered photonic crystal waveguides for optical delay lines," 6th IEEE International Conference on Group IV Photonics, 40-42 (2006).
26. C. Ciminelli, C.E. Campanella, F. Dell'Olio, and M.N. Armenise, "Fast light through velocity manipulation in two vertically-stacked ring resonators," Optics Express **18**, 2973-2986 (2010).
27. G. Lenz, B.J. Eggleton, C.K. Madsen, and R.E. Slusher, "Optical Delay Lines Based on Optical Filters," IEEE Journal of Quantum Electronics **37**, 525-532 (2001).
28. W. Shi, V. Veerasubramanian, D. Patel, and D.V. Plant, "Tunable nanophotonic delay lines using linearly chirped contradirectional couplers with uniform Bragg gratings," Opt. Lett. **39**, 701-703 (2014).
29. F. Morichetti, A. Melloni, A. Breda, A. Canciamilla, C. Ferrari, and M. Martinelli, "A reconfigurable architecture for continuously variable optical slow-wave delay lines," Optics Express **15**, 17273-17282 (2007).
30. F. Xia, L. Sekaric, and Y. Vlasov, "Ultracompact optical buffers on a silicon chip," Nature Photonics **1**, 65-71 (2007).
31. H. Tian, F. Long, W. Liu, and Y. Ji, "Tunable slow light and buffer capability in photonic crystal coupled-cavity waveguides based on electro-optic effect," Optics Communications **285**, 2760–2764 (2012).
32. F.M. Soares, F. Karouta, E. Smalbrugge, M.K. Smit, J. Lopez, A. Enard, and N. Vodjdani, "An InP-based photonic integrated beamformer for phased-array antennas," Integrated Photonics Research 2004, San Francisco, California United States, 30 June 2004.
33. P.A. Morton, J. Cardenas, J.B. Khurgin, and M. Lipson, "Fast thermal switching of wideband optical delay line with no long-term transient," IEEE Photonics Technology Letters **24**, 512-514 (2012).

34. C.T. Phare, Y.-H.D. Lee, J. Cardenas, and M. Lipson, "Graphene electro-optic modulator with 30 GHz bandwidth," Nature Photonics **9**, 511-515 (2015).

35. Y. Ding, X. Zhu, S. Xiao, H. Hu, L.H. Frandsen, N.A. Mortensen, and K. Yvind, "Effective Electro-Optical Modulation with High Extinction Ratio by a Graphene–Silicon Microring Resonator," Nano Letters **15**, 4393-4400 (2015).

36. V. Sorianello, M. Midrio, and M. Romagnoli, "Design optimization of single and double layer graphene phase modulators in SOI," Optics Express **23**, 6478-6490 (2015).

37. F. Bonaccorso, Z. Sun, T. Hasan, and A.C. Ferrari, "Graphene photonics and optoelectronics," Nature Photonics **4**, 611-622 (2010).

38. Q. Bao, and K. P. Loh, "Graphene Photonics, Plasmonics, and Broadband Optoelectronic Devices," ACS Nano **6**, 3677-3694 (2012).

39. H. Chang, and H. Wu, "Graphene-Based Nanomaterials: Synthesis, Properties, and Optical and Optoelectronic Applications," Advanced Functional Materials **23**, 1984-1997 (2013).

40. J. Capmany, D. Doménech, and P. Muñoz, "Graphene integrated microwave photonics," IEEE Journal of Lightwave Technology **32**, 3785-3796 (2014).

41. J.K. Thind, M. Kumar, and B.K. Kaushik, "Electrical tuning of optical delay in graphene-based photonic crystal waveguide," IEEE Journal of Quantum Electronics **51**, 6400105 (2015).

42. J. Capmany, D. Domenech, and P. Munoz, "Silicon graphene reconfigurable CROWS and SCISSORS," IEEE Photonics Journal **7**, 7050244 (2015).

43. W.A. Imbriale, S. Gao, and L. Boccia, *Space Antenna Handbook*, John Wiley & Sons (2012).

44. J.F. Bauters, M.J.R. Heck, D. John, D. Dai, M.-C. Tien, J.S. Barton, A. Leinse, R.G. Heideman, D.J. Blumenthal, and J.E. Bowers, "Ultra-low-loss high-aspect-ratio Si_3N_4 waveguides," Optics Express **19**, 3163-3174 (2011).

45. A. Gondarenko, J.S. Levy, and M. Lipson, "High confinement micro-scale silicon nitride high Q ring resonator," Optics Express **17**, 11366–11370 (2009).

46. D. Conteduca, F. Dell'Olio, C. Ciminelli, and M.N. Armenise, "Resonant Graphene-Based Tunable Optical Delay Line," IEEE Photonics Journal **7**, 1-9 (2015).

47. C. Ciminelli, D. Conteduca, F. Dell'Olio, M.N. Armenise, "Novel graphene-based photonic devices for efficient light control and manipulation," ICTON 2015, 17th International Conference on Transparent Optical Networks, Budapest, July 5-9, 2015, Invited paper.

48. V. Brasch, Q.-F. Chen, S. Schiller, and T.J. Kippenberg, "Radiation hardness of high-Q silicon nitride microresonators for space compatible integrated optics," Optics Express **22**, 30786-30794 (2014).

49. N. Gruhler, C. Benz, H. Jang, J.-H. Ahn, R. Danneau, and W.H.P. Pernice, "High-quality Si_3N_4 circuits as a platform for graphene-based nanophotonic devices," Optics Express **21**, 31678-31689 (2013).

50. S. Bae, H. Kim, Y. Lee, X. Xu, J.-S. Park, Y. Zheng, J. Balakrishnan, T. Lei, H. R. Kim, Y.I. Song, Y.-J. Kim, K.S. Kim, B. Özyilmaz, J.-H. Ahn, B.H. Hong, and S. Iijima, "Roll-to-roll production of 30-inch graphene films for transparent electrodes," Nature Nanotechnology **5**, 574-578 (2010).

51. T. Chen, H. Lee, and K.J. Vahala, "Design and characterization of whispering-gallery spiral waveguides," Optics Express **22**, 5196-5208 (2014).

52. E. Simsek, "A closed-form approximate expression for the optical conductivity of graphene," Opt. Lett. **38**, 1437–1439 (2013).